

Fin Ray Crossbeam Angles for Efficient Foot Design for Energy-Efficient Robot Locomotion

Poramate Manoonpong,^{*} Hamed Rajabi, Jørgen C. Larsen, Seyed S. Raoufi, Naris Asawalertsak, Jettanan Homchanthanakul, Halvor T. Tramsen, Abolfazl Darvizeh[†], and Stanislav N. Gorb

This article is dedicated to the memory of Prof. Abolfazl Darvizeh (1951–2021), who was a great mentor and colleague.

Robot foot and gripper structures with compliancy using different mechanical solutions have been developed to enhance proper contact formations and gripping on various substrates. The Fin Ray structure is one of the solutions. Although the Fin Ray effect has been proposed and exploited, no detailed investigation has been conducted on the effect of different crossbeam angles inside its frame. Thus, herein, an integrative approach is used, combining 3D printing with soft material, finite element modeling, and neural control to 1) manufacture the Fin Ray structure with compliancy; 2) investigate the effect of different crossbeam angles under different loads and cylindrical substrates; and 3) finally apply it as an efficient compliant robot foot structure for energy-efficient on-pipe locomotion. Considering the factors of a large contact area, high energy efficiency, and better durability, the Fin Ray model with nonstandard 10°-inclined crossbeams provides the best compromise in comparison with other models, within the constraints of the defined geometric parameters.

registered trademark of EvoLogics GmbH in some countries). He discovered the effect based on the studies of fish tailfin mechanics.^[1,2] When he applied a load to the fin, instead of bending outward, it bent inward against the applied load. This is due to the structure of the fish fin which consists of two bones connected to each other by elastic connective tissue. Kniese simplified the biomechanical structure into a triangular frame with crossbeams stacked one above the other ($\theta = 90^\circ$, **Figure 1a**). The beams connect the left and right bars of the frame, where the base is wider than the tip. The simplified structure reacts to an applied load by moving its tip against the load (**Figure 1b**).

Due to this interesting mechanism, the Fin Ray effect has been analyzed and used in various applications,^[1,3–12] primarily the

1. Introduction

In 1997, Leif Kniese, biologist, introduced the Fin Ray effect which was later patented by EvoLogics GmbH (Fin Ray is a

design of robot grippers (**Figure 1c**). For example, the company Festo developed the MultiChoiceGripper using the traditional Fin Ray-based structure (**Figure 1c**) for passive adaptable object grasping.^[3] Shan and Birglen presented a detailed mathematical

P. Manoonpong, J. C. Larsen
Embodied AI and Neurorobotics Lab
SDU Biorobotics
The Mærsk Mc-Kinney Møller Institute
University of Southern Denmark
Campusvej 55, Odense M 5230, Denmark
E-mail: poma@mmmi.sdu.dk

P. Manoonpong, N. Asawalertsak, J. Homchanthanakul
Bio-inspired Robotics and Neural Engineering Lab
School of Information Science and Technology
Vidyasirimedhi Institute of Science and Technology
555 Moo 1 Payupnai, Wangchan, Rayong 21210, Thailand

H. Rajabi, H. T. Tramsen, S. N. Gorb
Department of Functional Morphology and Biomechanics
Zoological Institute
Kiel University
Am Botanischen Garten 1-9, D-24098 Kiel, Germany

H. Rajabi
Division of Mechanical Engineering and Design
School of Engineering
London South Bank University
103 Borough Rd, London SE1 0AA, UK

S. S. Raoufi, A. Darvizeh
Department of Mechanical Engineering
Bandar Anzali Branch, Islamic Azad University
Talibabad, Bandar-e-Anzali 43131-11111, Iran

 The ORCID identification number(s) for the author(s) of this article can be found under <https://doi.org/10.1002/aisy.202100133>.

© 2021 The Authors. Advanced Intelligent Systems published by Wiley-VCH GmbH. This is an open access article under the terms of the Creative Commons Attribution License, which permits use, distribution and reproduction in any medium, provided the original work is properly cited.

[†] A. Darvizeh passed away, just before the manuscript was submitted for publication

DOI: 10.1002/aisy.202100133

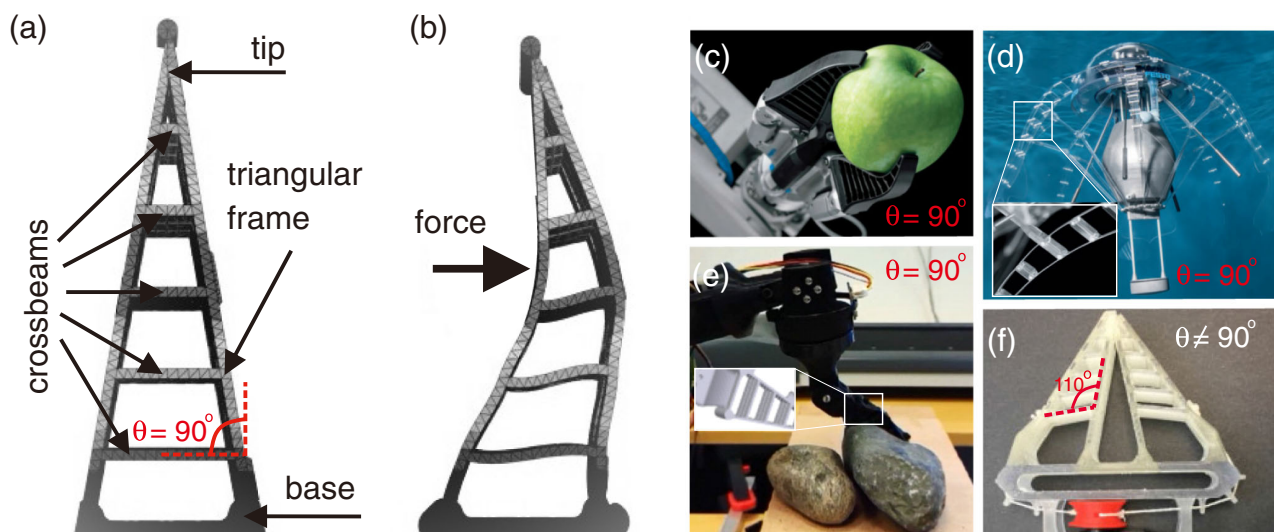


Figure 1. The characteristics of the Fin Ray effect and its applications. a) The Fin Ray structure without a load. b) The Fin Ray structure with an applied force. c) Festo MultiChoiceGripper. Reproduced with permission.^[3] Copyright Festo SE & Co. KG, all rights reserved. d) Festo AquaJelly (artificial jellyfish). Reproduced with permission.^[4] Copyright Festo SE & Co. KG, all rights reserved. Zoom panel is the standard Fin Ray-based structure in the AquaJelly tentacles. e) Bio-inspired compliant tarsus (i.e., robot foot).^[5] Zoom panel is the standard Fin Ray-based structure in the foot. Reproduced with permission.^[5] Copyright 2016, Springer Nature. f) Tufts passive gripper with a nonstandard Fin Ray-based structure. Reproduced with permission.^[6] Copyright 2017, The Author(s). Published by SAGE Publications.

modeling and performance analysis of parallel grippers equipped with soft fingers based on the Fin Ray effect with traditional inclined crossbeams of 90° .^[13] In addition to the Fin Ray-based robot grippers, the Fin Ray structure was also applied to build flexible limbs (part of the body) of the AquaJelly (artificial jellyfish, Figure 1d). This enables it to perform the natural swimming movements like the jellyfish.^[4] Di Canio et al. used the Fin Ray structure as a robot foot to allow the legged robot to walk on curved surfaces^[5] (Figure 1e). In these gripper, body/limb, and foot designs, the traditional Fin Ray structure ($\theta = 90^\circ$, Figure 1a,b) is used, as it is symmetric and capable of bending equally in either direction.

Recently, Crooks et al. proposed a robot gripper using a modified asymmetric Fin Ray structure with inclined crossbeams of 110° from the inner frame^[6] (Figure 1f). The special gripper only requires power to open and close and does not need any additional power to maintain the grip. Chen et al. took the concept further to develop bio-inspired and shape-adaptive soft robotic grippers (SRGs) augmented with electroadhesion (EA) functionality. The gripper basically combines a Fin Ray structured two-fingered SRG with two soft-stretchable EA pads. The crossbeams of the Fin Ray structure were also optimized, resulting in a small inclined angle from the base. The gripper can effectively grasp and lift deformable and delicate objects due to the inclined crossbeams and the utilization of the EA functionality.^[14] Elgeneidy et al. optimized limited number of soft fingers based on the Fin Ray effect to reach minimal initial contact forces to interact with delicate objects and a maximal force when used in high-force applications.^[15] The optimization was based on asymmetry by increasing the angles of the first beam (from 10° to 25°) and the successive beams (from 0° to 3°) with respect to the base. All these technical findings have pointed out that the gripping performance of the traditional Fin Ray structure can be enhanced by

introducing the slope angle of the crossbeams ($\theta \neq 90^\circ$, e.g., Figure 1f). There are also evidences in nature supporting the findings (Figure 2). Many animals are able to carry out effective gripping or attaching actions to the surfaces using compliant pads on their limbs where compliancy is based on multiple angled crossbeams within the material.

These pads often consist of a very flexible superficial layer, which due to its compliance can adapt to the substrate profile during contact formation, thereby maximizing the real contact area (RCA) with the substrate. Such structures have been described in animals belonging to different lineages, such as insects,^[16–18] tree frogs,^[19,20] bats,^[21,22] and echinoderms.^[23,24] Independent from the basic physical mechanism of adhesion and friction, the superficial layer of pads always exhibits a rather similar inner structure of a fibrous nature. These fibers/struts/crossbeams are connected to a stiffer supporting layer on one side and terminated by flexible layers on the other, and thus resemble the Fin Ray structure. However, the fibers in the majority of the aforementioned biological systems are never oriented perpendicularly to the substrate (as in the regular Fin Ray), but rather at various slope angles (Figure 2). One reason for such structure might be the resulting softness of the overall system, which allows for compensation of the surface roughness.^[25,26]

Inspired by the technical findings^[6,14,15] and biological evidences^[16,27,28] of the nonperpendicular orientation of crossbeams/fibers of the Fin Ray-like structure (Figure 1f and 2), in this study, we further investigate the mechanical behavior of such a system combining finite elements analysis (FEA) with an experiment involving 3D-printed compliant Fin Ray structures under different crossbeam angles. We also investigate the effect of different angles on nonflat substrate gripping for energy-efficient robot locomotion. To the best of our knowledge, a detailed investigation on the effect of different crossbeam angles of the Fin Ray

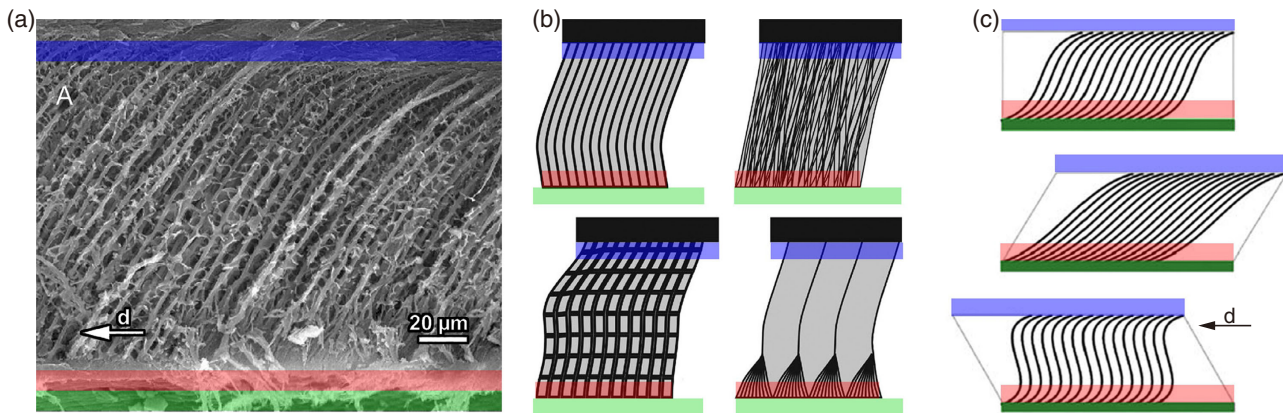


Figure 2. Fin Ray-like contact systems in biology. a) Section through the smooth attachment pad of the bush cricket *Tettigonia viridissima*, scanning electron microscope (SEM) micrograph. Adapted with permission.^[16] Copyright 2000, The Royal Society. b) Scheme of internal architecture of various smooth attachment pads of insects: generic fiber-like type found in most pads (right above); thin filamentous type of honey bee (Hymenoptera) (left above); foam-like type found in cicada (Auchenorrhyncha) (right below); hierarchical type found in bush crickets (Orthoptera) shown in a (left below). Adapted with permission.^[28] Copyright 2006, Elsevier. c) Hypothetical scheme of the fiber alignment within the attachment pads, depicted in a and b, under different shear conditions in contact with substrate (no shear, backward shear, and forward shear). Adapted with permission.^[16] Copyright 2000, The Royal Society. Blue, rigid support; green, rigid substrate; and red, flexible terminal surface film.

structure proposed here has not been fully addressed. For possible bio-inspired technical applications in robotics, it is important to understand the role of the slope angle of fibers/struts in achieving proper contact formation on nonflat substrates. Taken together, our study has two main objectives: 1) to carry out a detailed investigation; and 2) to identify proper nonstandard crossbeam angles for the design of a robot foot which will lead to good contact formation (grip) and force transmission to the substrate for energy-efficient locomotion (a basis for machine intelligence).

2. Results

2.1. The Effect of Different Crossbeam Angles in the Fin Ray

Here, using FEA-based numerical simulation, we investigate the effect of different crossbeam angles on the deformability of a compliant Fin Ray-based structure. The developed models with different crossbeam angles including a typical angle of 90° (Figure 3a) were subjected to two loading scenarios (Figure 3b): 1) a constant load of 5.4 N applied by cylinders with different dimensions; and 2) different loads applied by the same cylinder with a radius of 4 cm. The results of the first loading scenario are shown in Figure 2c. As can be seen here, increasing the size of the cylinders also increased the contact area between the Fin Ray models and cylinders. For the cylinders with the middle sizes ($r = 2$ and 3 cm), the crossbeam angles of 30° and 120° always resulted in the two greatest contact areas. While the small and large sized cylinders ($r = 1$ and 4 cm), the crossbeam angles of 120° and 10° resulted in the greatest contact area, respectively.

Figure 3d shows the results of the second loading scenario. As can be seen here, while an applied load of 0.54 N leads to only very little contact between the Fin Ray models and cylinder, increasing the applied load also increased the contact area when the size of the cylinder was kept constant. Here, the contact area was greatest for

models with crossbeam angles of 10°, 30°, and 120° at the middle and large applied loads (2.7 and 5.4 N). To verify the validity of our numerical simulation results, we carried out real physical tests. Several compliant Fin Ray models were 3D printed from a combination of the FilaFlex filament (elastic filament for 3D printers) and PLA filament (see also the Experimental Section) and subjected to a loading similar to one of those used in the numerical analysis. Figure 3e shows four representative examples to compare the deformation of the numerical and physical models. A detailed comparison is shown in Table S1, Supporting Information. The comparison shows very similar deformation behavior for both model groups under similar loading conditions. While the accuracy of the numerical models in predicting the contact area of Fin Ray models varies according to changes in the crossbeam angles (see Table S1, Supporting Information), an average error of 4.3% indicates good overall performance. To identify not only the deformability (shown earlier) but also durability of different crossbeam angles, we also measured the maximum principal stress within the models when subjected to loading (Figure 4).

Here, the stress is shown for four Fin Ray models with crossbeam angles of 10°, 30°, 90°, and 120° under two loading conditions: 1) when subjected to a 5.4 N load applied by cylinders of different sizes (radii of 1, 2, 3, and 4 cm) (Figure 4a); and 2) when subjected to different loads (0.54, 2.7, and 5.4 N) using a cylinder with a radius of 4 cm ($r = 4$ cm, Figure 4b). While the stress within the models varies according to changes in the loading scenario, the Fin Ray model with the 30° crossbeam angle always exhibited the maximum amount of stress. Under the largest applied load (5.4 N, Figure 4a), the models with crossbeam angles of 10° and 120° showed lower stress levels on average (better durability) in comparison with the model with a crossbeam angle of 90°, except for $r = 2$ and 4 cm in which the stress in the models with crossbeam angles of 10° and 120° are almost equal to the one of 90°, respectively. Figure 4c shows the distribution of stress within the models when subjected to a 2.7 N load

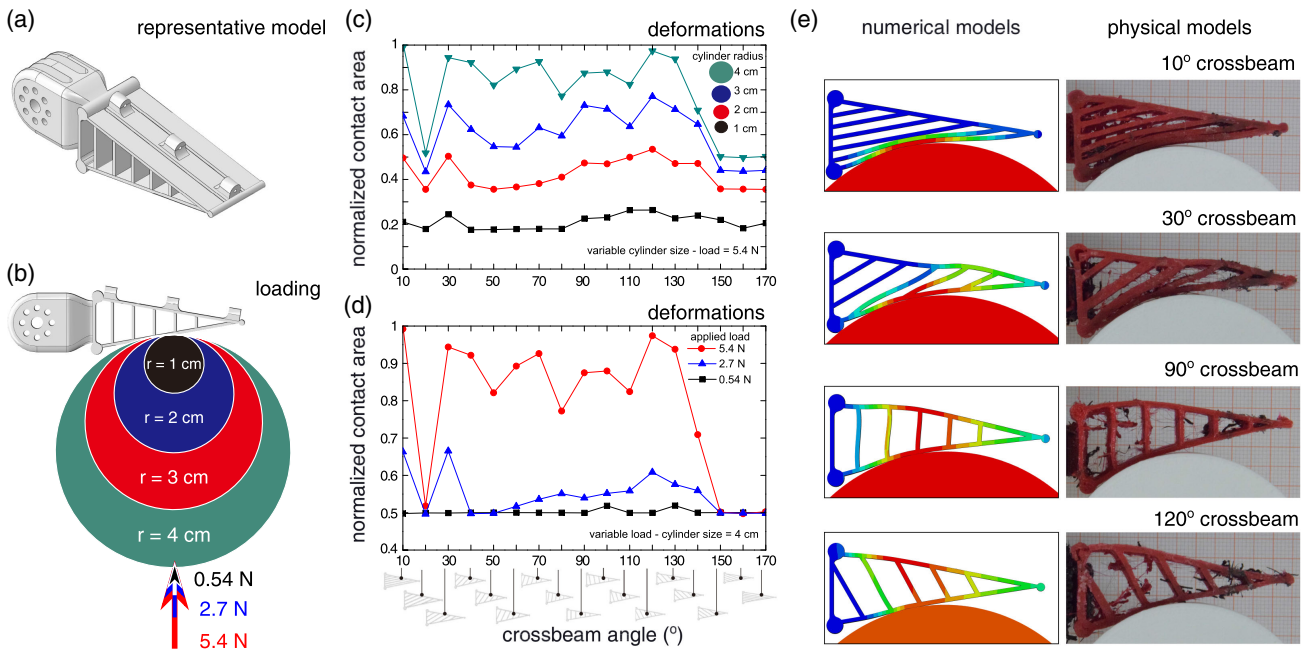


Figure 3. Deformations of Fin Ray models with different crossbeam angles under loading. a) A representative Fin Ray model with a crossbeam angle of 90°. b) The models were investigated under two loading scenarios. In the first loading scenario, the models were subjected to a constant load of 5.4 N using four cylinders with different radii. In the second scenario, the models were subjected to different loads using the same cylinder with a radius of 4 cm. c) The area between the Fin Ray models in contact with cylinders with different radii (the applied load (5.4 N) was kept constant). d) The contact area between the Fin Ray models under different applied loads (the size of the cylinder (4 cm radius) was kept constant). In both loading scenarios, the Fin Ray models with crossbeam angles of 10°, 30°, and 120° had a comparatively large contact area with the cylindrical substrates in most of the cases. The results in (c) and (d) were obtained from FEA-based numerical simulation. Note that, a normalized contact area was calculated by subdividing each contact area to the maximum obtained contact area. e) Comparison of the results from numerical simulations and physical experiments. Representative results are shown for crossbeam angles of 10°, 30°, 90°, and 120°. Both simulations and experiments were conducted under a load of 2.7 N, applied using a cylinder with a radius of 4 cm.

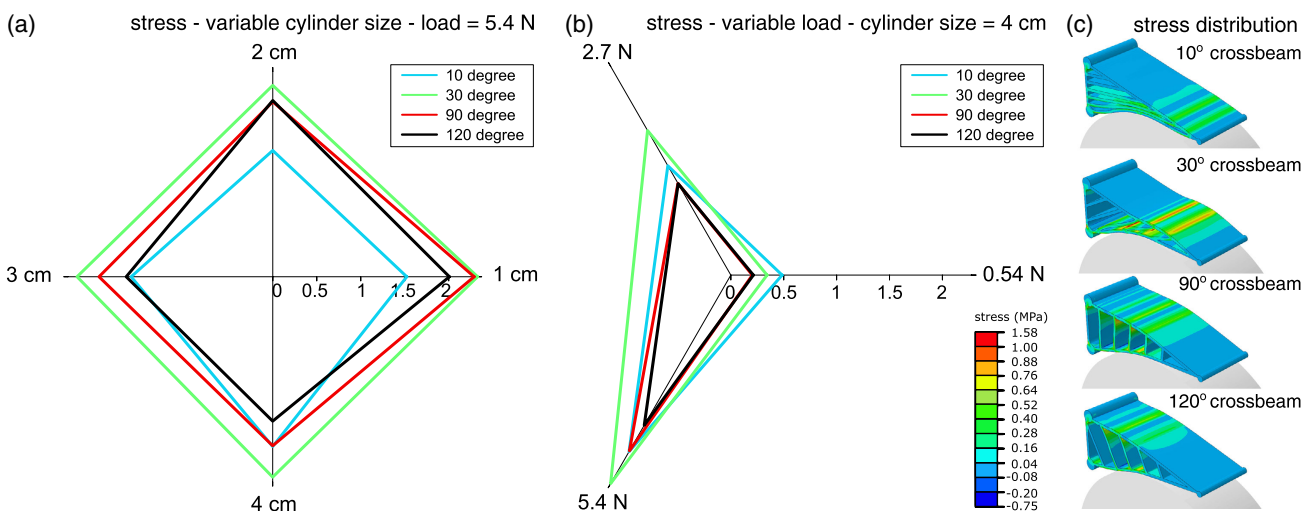


Figure 4. Maximum principal stress in the selected models. a) Maximum stress in the models with crossbeam angles of 10°, 30°, 90°, and 120° subjected to a 5.4 N load applied using cylinders with different radii of 1, 2, 3, and 4 cm. b) Maximum stress in the models with crossbeam angles of 10°, 30°, 90°, and 120° subjected to 0.54, 2.7, and 5.4 N loads applied by a cylinder with a radius of 4 cm. c) Distribution of the stress in selected models under the 2.7 N load applied by a cylinder 4 cm in radius.

applied by a cylinder with a radius of 4 cm. Regions with relatively high levels are indicated in yellow and red. These are particularly apparent in the case of the models with crossbeam angles of 30° and 90° resulting in low durability.

2.2. Compliant Fin Ray-Based Robot Foot Structure for Energy-Efficient Locomotion

In addition to the experiments with the pure Fin Ray-based structure described earlier, we also carried out real robot locomotion experiments using a three-jointed bio-inspired robot leg equipped with a 3D-printed Fin Ray model as its foot (Figure 5a). The total weight of the leg and foot is ≈ 275 g or 2.7 N. The leg was attached to a moving cart, constrained by two rails. This is to ensure that the leg walks along a given path (Figure 5). The leg was driven by neural locomotion control (see the Experimental Section). Figure 5b–e shows motor control signals generated by the control and one walking cycle of the leg, respectively. For the walking pattern, the first (TC) and second (CF) joints rotate periodically, whereas the third (FT) joint is set to a certain angle.

We used four different Fin Ray-based foot structures with different crossbeam angles for the experiment. One is the original Fin Ray with 90° inclined crossbeams, whereas the other three have 10°, 30°, and 120° inclined crossbeams. The 10°, 30°, and 120° inclined crossbeams were selected as they are the three largest deformations at a load of ≈ 2.7 N (see blue line in Figure 3d). Figure 6a shows a comparison of specific resistances^[29] of the leg

with different crossbeam angles of the foot during locomotion on a 4 cm radius cylindrical tube. A detailed statistical test is shown in Table S2, Supporting Information.

The specific resistance ϵ or cost of transport (COT) is the ratio between the consumed energy and the transferred gross weight multiplied by the distance traveled: $\epsilon = E/mgd$, where E is energy, mg is the weight of the leg (2.7 N), and d is the distance traveled (in this case, 80 cm). The energy is estimated from: $E = IVt$. I is the average electric current in amperes used by the motors of the leg when walking at a distance of 80 cm, measured using the Zap 25 current sensor. V is voltage (in this case, 5 V). t is time in seconds for the distance traveled (i.e., we precisely measure the timing at which the robot reached 80 cm). Low ϵ corresponds to highly energy-efficient walking.

The results show that the foot with 10° and 30° inclined crossbeams leads to, on average, low specific resistance; thereby achieving more energy-efficient locomotion compared with those with the traditional Fin Ray having 90° inclined crossbeams and the one having 120° inclined crossbeams. This is because the foot with the 10° and 30° crossbeams are more flexible and can deform more easily; thereby increasing the contact area between the foot and the substrate (Figure 6b,c). The contact areas of the 90° and 120° crossbeams measure 5 and 6.8 cm², respectively, whereas those of the 10° and 30° crossbeams are 8 and 7.4 cm² which are 37.5% and $\approx 32\%$ more than the 90° crossbeams and 15% and $\approx 8\%$ more than the 120° crossbeams, respectively.

Based on the single-leg experiments, we further validated the performance of the Fin Ray-based foot structure on hexapod

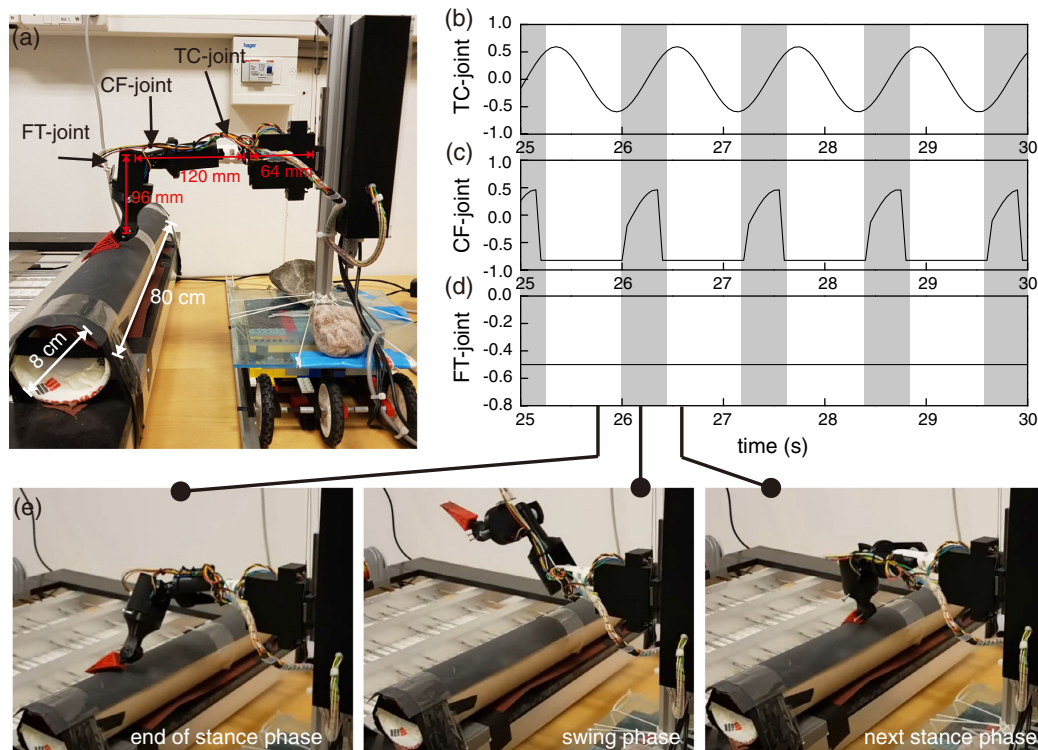


Figure 5. Bio-inspired robot leg with a compliant Fin Ray-based foot and its walking behavior. a) The setup of the leg with a cart to evaluate locomotion efficiency on a cylindrical tube. b–d) Motor signals of the leg during walking. White areas indicate a stance phase (i.e., the foot touches the tube) and gray areas refer to a swing phase (i.e., the foot is in the air). e) Snapshots of locomotion of the leg during the experiment.

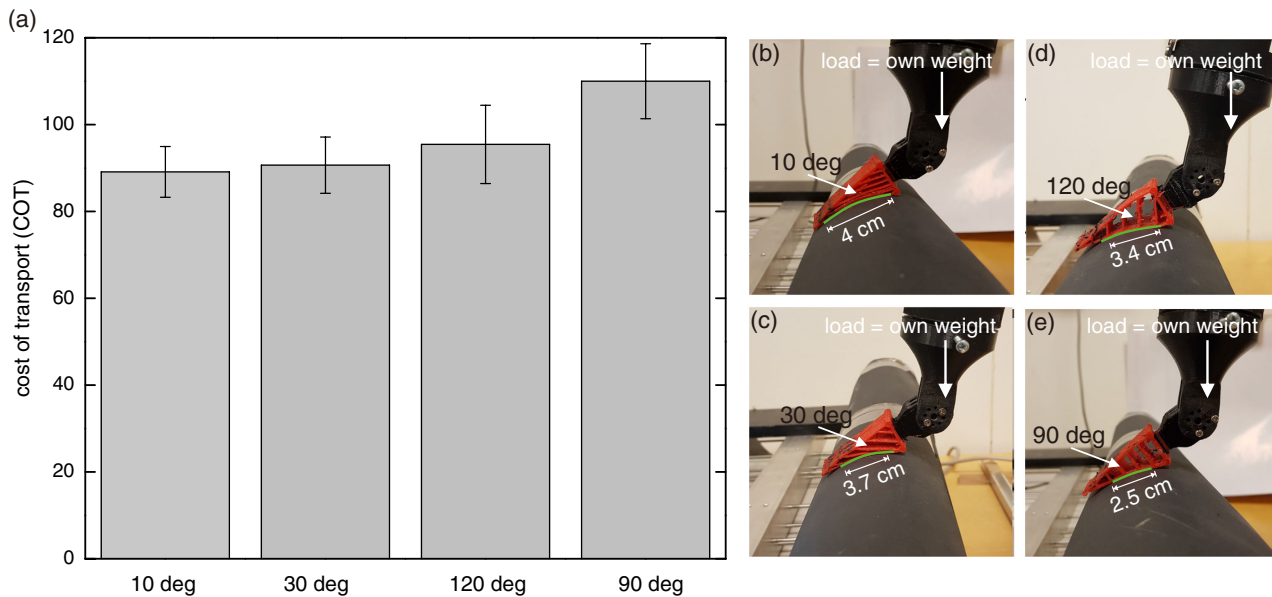


Figure 6. Results of the walking experiment of the single-legged robot with a compliant Fin Ray-based foot. a) A comparison of average cost of transport (COT) of the foot with different crossbeam angles (10°, 30°, 90°, and 120°) during locomotion on the tube. The standard deviation shows the variance for five runs each. b–e) The contact areas (highlighted in green) between the tube surface and the different types of foot. In this case, the leg was placed on the tube and its own weight applied to it (≈ 2.7 N). A video showing the locomotion of the leg with a Fin Ray-based foot with 10°, 30°, 90° (classical), and 120° crossbeam angles can be viewed at Video S1, Supporting Information, or <http://www.manoonpong.com/FinRay/VideoS1.mp4>.

robot walking experiments (Figure 7). Here, we used 10° Fin Ray-based feet as this angle shows the greatest contact area to the curved surface compared with the other angles (Figure 6). We installed the feet on the robot (Figure 8d) and let it walk at a distance of 90 cm on two different surfaces: curved surface (parallel 6 cm diameter pipes, Figure 7a) and loose rocky surface (gravel terrain, Figure 7e). We applied neural locomotion control without sensory feedback (Figure 8) to drive robot locomotion with a wave gait (Figure S1, Supporting Information) and measured the COT. We compared the COT of the 10° Fin Ray-based feet with hemispherical rubber feet (Figure 7d,h). The hemispherical rubber feet are standard feet typically used for walking robots. The result shows that the robot with the standard rubber feet failed to walk on the pipes (Figure 7c), whereas the robot with the Fin Ray-based feet was able to walk on the pipes and complete the track in all five runs (Figure 7b). For walking on the gravel terrain, the result shows that using the Fin Ray-based feet leads to lower COT (more energy-efficient locomotion) than using the standard feet (Figure 7h). Furthermore, walking with the Fin Ray-based feet results in less deviation from the straight path compared with the standard feet (Figure 7f,g). Unlike standard feet, the Fin Ray-based feet can passively adapt to the surfaces to increase the contact area between the legs and the surfaces. This allows the robot to maintain a stable grip on the surfaces during the stance phase, which improves locomotion.

It is important to note that, while the foot design with the 10° crossbeams can significantly increase the contact area between the leg and curved substrate, in the single-leg experiments, we observed that the foot still showed small slipping at the end of stance (Figure 5e and Video S1, Supporting Information).

This can be improved by, e.g., adding a torsional spring in its connection between the leg and the foot to allow the sole of the foot to remain parallel to the surface.^[30] Applying a large load is another way to reduce or prevent slipping. This is demonstrated in the hexapod robot walking experiments. The total weight of the robot is ≈ 4 kg or ≈ 39 N. During a stance phase with this weight, each leg received a large applied load of ≈ 6 – 8 N (robot own weight), preventing foot slipping (Figure 7b and Video S2, Supporting Information).

3. Discussion

Through our numerical and physical models, we found that, within the framework of the geometric parameters considered here, there are three main crossbeam angles (i.e., 10°, 30°, and 120°, Figure 3), which produce greater contact between the Fin Ray and the substrate. This is because these crossbeam angles allow higher deformability of the Fin Ray structure, compared with the other angles including the typically used crossbeam angle of 90°. Furthermore, our investigation also shows that as an applied load significantly increases (e.g., 5.4 N), the contact areas of 10° and 120° also significantly increase resulting in a good grip (Figure 3d). Thus, they are the best candidates among the other angles if a large load is a key factor. As a radius of cylinder significantly increases or curvature decreases (e.g., 4 cm), the contact area of 10° significantly increases (Figure 3c), so that it reaches the greatest contact area among all. For all radii, a crossbeam angle of 120° shows an overall large contact area. Therefore, a crossbeam angle of 120° is a good candidate for robotic applications that will deal with the variations of load and curvature; whereas a crossbeam angle of 10° is a good

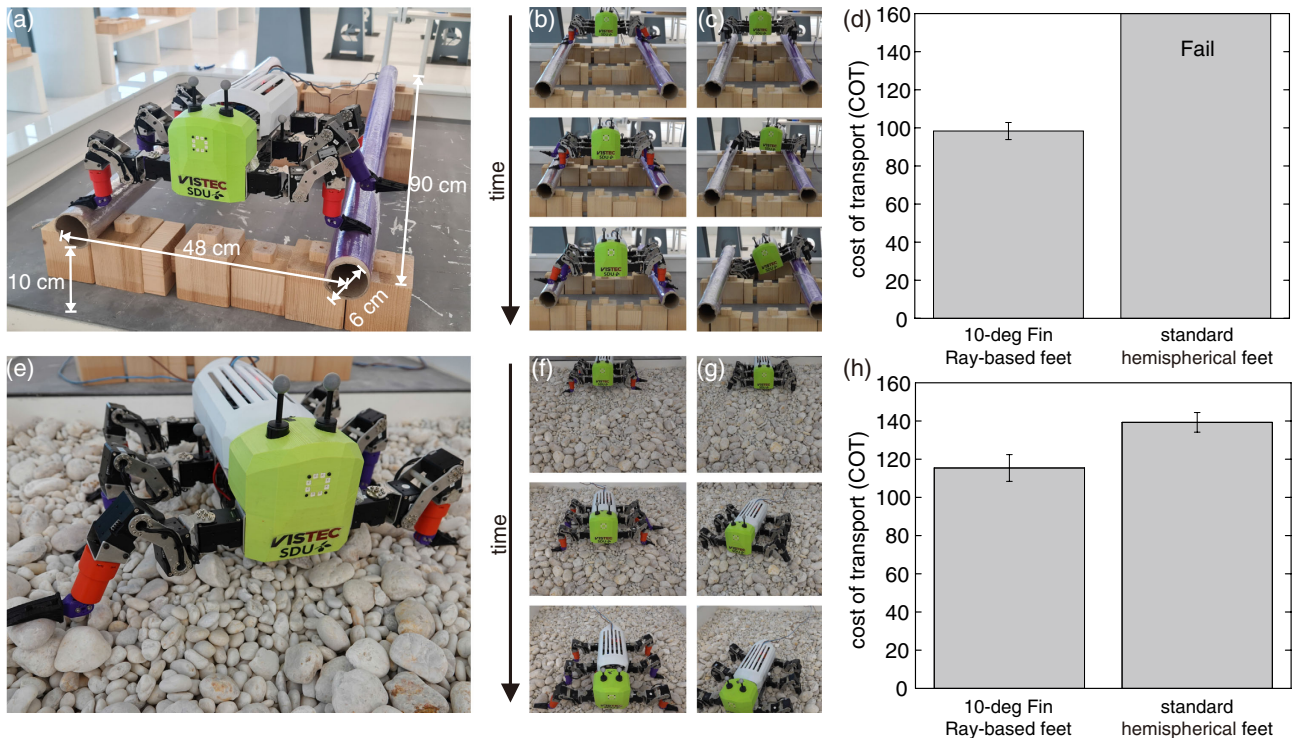


Figure 7. Results of the walking experiment of the hexapod robot with compliant Fin Ray-based feet. a) The setup of the hexapod robot walking on 6 cm diameter pipes. b) Walking on the pipes with 10° Fin Ray-based feet (from top to bottom). c) Walking on the pipes with standard hemispherical rubber feet (from top to bottom). d) A comparison of average COT of the Fin Ray-based and standard feet during locomotion on the pipes. The standard deviation shows the variance for five runs each. e) The setup of the hexapod robot walking on gravel terrain. f) Walking on the terrain with the Fin Ray-based feet (from top to bottom). g) Walking on the terrain with the standard feet (from top to bottom). h) A comparison of average COT of the Fin Ray-based and standard feet during locomotion on the terrain. The standard deviation shows the variance for five runs each. A video of the experiment can be viewed at Video S2, Supporting Information, or <http://www.manoonpong.com/FinRay/VideoS2.mp4>.

candidate for those that will experience a large applied load and interact with a large radius pipe (as shown in Figure 6 and 7). These results suggest that changing the orientation of the crossbeam angles can help to fine tune the deformability of the Fin Ray structures. This strategy can enhance the performance of such structures when used as robot feet (Figure 6 and 7) or grippers (Figure S2, Supporting Information). To validate this claim, we carried out single-leg experiments using four different crossbeam angles: the structurally optimal angles of 10°, 30°, and 120° as well as the typical 90° angle (Figure 5). Our robot experimental results show that the crossbeam angles of 10° and 30° lead to almost equally high energy-efficient locomotion (Figure 6) where the 10° angle shows the greatest contact area (Figure 6b). In contrast, the crossbeam angle of 120° shows lower energy efficiency, although still higher than the typical 90° angle. In addition, we demonstrate the application of the Fin Ray-based foot structure with 10° inclined crossbeams for efficient hexapod walking on parallel pipes and gravel terrain.

The stress analysis of the numerical models, in contrast, show notably higher stress levels in the model with the crossbeam angle of 30°, compared with the other models (Figure 4). The high stress level reduces the durability of this model and increase the risk of failure under high loads. Hence, considering the factors of a large contact area (resulting in a good grip), high energy efficiency, and better durability, the compliant Fin Ray model

with a crossbeam angle of 10° is likely to provide the best compromise in comparison to other models under a high load and a large cylindrical substrate. Note that, tribological studies have revealed that a structure with compliance shows shape adaptation which can increase the real contact area (RCA) with the substrate; thereby increasing friction at the same load compared with a rigid one.^[31–33] As a consequence, the force of friction (gripping force) is also increased. The effect of RCA based on a compliance model is different from a classical contact model which is independent of apparent contact area (ACA). The Fin Ray-based foot with a special crossbeam angle (here 10°) follows the principle of RCA and generates strong RCA due to its specific compliancy and contact behavior; thereby creating a higher friction for a better grip.

In walking robot development, different foot structures have been developed for locomotion enhancement.^[34–37] For example, Ohtsuka et al.^[35] developed the terrain adaptive foot for the quadruped walking robot TITAN VIII. The foot mechanism is composed of a deformation mechanism with four fingers, a shape-fixing mechanism, and a vertical force sensor. With this foot mechanism, the robot can walk on uneven terrain. Voigt et al.^[38] developed an active robot foot with foamy rubber materials for the small robot Ratnic. It acts as a gripper with specific movement control for climbing on a pipe. Hauser et al.^[36] applied the method of jamming of granular media in

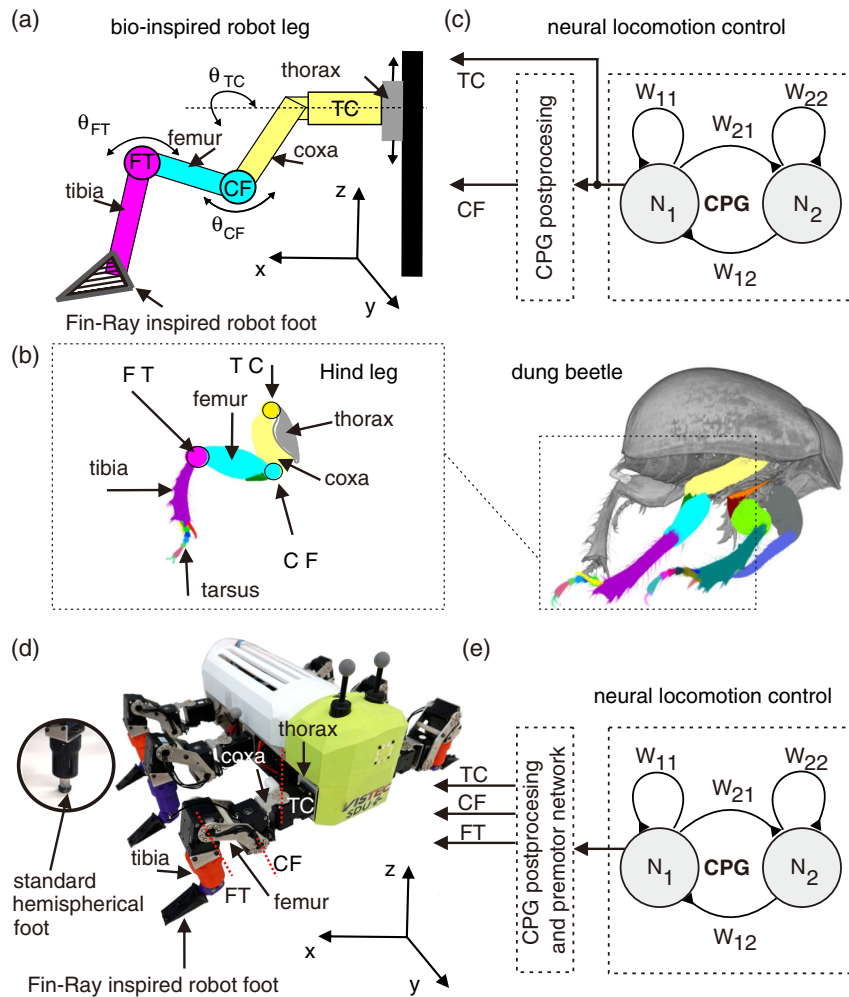


Figure 8. Bio-inspired robots with a Fin Ray-based foot structure and neural locomotion control. a) Schematic diagram of the dung-beetle like robot leg with a Fin Ray-based foot. b) 3D scanned image of a dung beetle (posterolateral view). The right zoom panel shows its segmented hind leg being used as a model to develop the robot leg. c) CPG-based neural locomotion control of the leg. It consists of a CPG module and a CPG postprocessing module. The CPG module has two interconnected neurons $N_{1,2}$. The periodic output of the neuron N_1 directly drives the TC joint and indirectly drives the CF joint through a CPG postprocessing module, whereas the FT joint remains fixed. This leads to a stepping pattern of the leg. d) Hexapod robot with Fin Ray-based feet. The circle inset shows a standard rubber foot of walking robots used for a comparison. e) CPG-based neural locomotion control of the hexapod robot. It consists of a CPG module based on two interconnected neurons $N_{1,2}$, a CPG postprocessing module, and a premotor network module. The periodic outputs of the neurons $N_{1,2}$ are translated through CPG postprocessing and premotor network modules into proper motor signals controlling all TC, CF, and FT joints and forming a walking pattern.

universal grippers to build compliant feet on a four-legged robot. The feet are actively controlled to switch between two states (a soft state, where granules can move freely, and a hard state, where the granules are locked in an arrangement) for walking on uneven and curved surfaces. In general, the use of granular media-based compliant pads can improve robot performance on a wide variety of natural substrates.^[39] Recently, Paez et al.^[37] proposed adaptive compliant foot design for salamander robots. The foot consists of three fingers actively controlled by one motor. This concept is in line with the multichain system of the insect tarsus, allowing great universality during locomotion on a wide variety of substrates.^[40] Based on the concept, the foot can adapt to an abrupt change in the terrain, e.g., stepping on a rock. While

all these foot designs show impressive performance in their own right, they still require complex mechanisms and/or active control.

In contrast, our proposed efficient compliant Fin Ray-based robot foot structure requires neither complex mechanisms nor active control. It can passively adapt to surface contour (particularly curved surfaces) using its flexible structure and soft material; thereby increasing the contact area between the leg and substrate for efficient locomotion. This development strategy without active (complex) control follows the concept of morphological computation; i.e., by exploiting physical intelligence (such as structure and material) and interaction with the environment, we can reduce control effort. In other words, we offload the complex control to body intelligence.^[41,42] In fact, the efficient Fin

Ray-based structure can be also used as a robot arm gripper (Figure S2, Supporting Information). Due to the structure's passive adaptability, the gripper can grasp a variety of (soft) objects, including those that are fragile (Figure S2 and Video S3, Supporting Information or <http://www.manoonpong.com/FinRay/VideoS3.mp4>).

4. Conclusion

In this study, we show for the first time, a detailed investigation of the deformability of a well-known Fin Ray-based structure with compliancy at different crossbeam angles. Although the Fin Ray effect has been proposed and exploited in a number of robotic applications (e.g., robot gripper, foot, and body/limb), a detailed investigation shown here has not yet been performed. Our findings show that the Fin Ray models with certain nonstandard inclined crossbeams can exhibit an enhanced compliance and deform more easily than other models (including the traditional model with 90° inclined crossbeams); thereby increasing the contact area between the model and surface. Furthermore, some of these models can also provide a better compromise in comparison to other models in terms of high energy efficiency and better durability (low stress) which will reduce risk of failure in practice. We also demonstrate that using the Fin Ray model with a proper crossbeam angle (in this case and within the geometric parameters used here, 10°) as an efficient compliant Fin Ray-based robot foot structure with soft material can enhance robot locomotion efficiency and even increase its field of operation (in this case, on a pipe or parallel pipes) without further need for complex control and sensory feedback.

To this end, this study originally provides the following contributions. 1) It shows the effects of different crossbeam angles in the Fin Ray structure; 2) It proposes a novel approach that uses the structure (compliant Fin Ray-based foot) with proper crossbeam angles to automatically improve grip with the curved substrate instead of using soft (foam rubber^[38]) or sticky (scotch tape^[43]) materials as typically used by existing approaches. This efficient structural design approach (i.e., morphological computation) can avoid wear and contamination which usually occur for soft or sticky materials;^[38,43] 3) It demonstrates energy-efficient pipe walking of bio-inspired legged robots with the efficient foot structure; 4) It suggests an insight into the identification of proper crossbeam angles for other robotic applications, such as curved-object grasping. Finally, 5) it encourages "roboticist rethinking" using Fin Ray structures with proper crossbeam angles in the future development of energy-efficient robot motion as a basis for machine intelligence.

As this work here is a comparative study where we used common flexible material for 3D printed deformable foot structures, we hypothesize that our results should hold true when changing foot material but still using the sufficiently stiff substrate. However, a further investigation of material properties (modulus, Poisson's ratio, stress, and stain) of the 3D printed foot is required to address the hypothesis. Another promising direction for future research is the investigation of the dependency of the optimal crossbeam angles to the geometric parameters of Fin Ray structures, such as length, width, number of crossbeams, their thickness, etc. Future studies can also investigate the effect

of layer jamming on the mechanical response of Fin Ray structures. This happens when, due to the large deformation of the Fin Ray structure, the adjacent crossbeams contact each other and, thereby, its stiffness increases. This is the reason that the Fin Ray structure with 20° inclined crossbeams made a noticeably smaller contact area with the substrate than others (Figure 3c,d).

In principle, this foot design can also be used simultaneously as a gripper for grasping an object. Therefore, the implementation of such feet on legs allows the robot to use its legs for locomotion on different surfaces^[5] including curved and rocky (shown here), as well as object manipulation/transportation. We believe that this study can also be a basis for future robot development and will open up the opportunity for practical robotic applications requiring robot locomotion on terrain with various convexities (or various pipe diameters), such as pipe inspection in the oil and gas industry.

5. Experimental Section

Modeling of Compliant Fin Ray-Based Structures: Here, we investigated the effect of different crossbeam angles on the deformability of a Fin Ray-based structure. To do so, we first modeled a set of Fin Ray-based models with varying crossbeam angles from 10° to 170° at 10° intervals. All the models were developed using the commercial finite element (FE) software package ABAQUS (v.6.14; Simulia, Providence, RI, USA). The models had a length, width, and height of 45, 20, and 20 mm, respectively. Figure 2a shows one of the models with 90° crossbeams with respect to a horizontal line. General-purpose eight-node solid elements with reduced integration (C3D8R) were used to mesh the developed models.

The reduced-integration scheme makes these elements suitable for simulating the mechanical behavior of rubber or elastic-like (soft) materials with large deformability. The material properties of the Fin Ray-based models were considered to be similar to those of physical models (Figure 3e and Table S1, Supporting Information) in terms of a density of 1200 kg m⁻³, an elastic modulus of 48 MPa, and a Poisson's ratio of 0.35. The cylinders were modeled as complete rigid structures with no deformability. All the Fin Ray-based models were fully fixed at their basal handle, designed to be screwed to a robot leg. The Fin Ray-based models were subjected to two loading scenarios. In the first scenario, we developed cylinder models with four different radii, ranging from a small cylinder with a radius of about one-quarter of the Fin Ray length to a large cylinder with a radius almost equal to the Fin Ray length (i.e., 1, 2, 3, and 4 cm). We used the cylinders to apply a normal load of 5.4 N to the bottom of the Fin Ray models (Figure 3b).

In the second loading scenario, we chose the largest cylinder model (with a radius of 4 cm), to better represent the irregularity of the pipe on which a robot walks (Figure 5), and used it to apply three different normal loads to our Fin Ray models. The loads were chosen to cover a magnitude corresponding to the proportionate weight of one leg of small- to medium-scale legged robots (i.e., 0.54, 2.7, and 5.4 N). The developed models enabled us to simulate their deformation under the two loading scenarios. The results were used to measure the area of contact between the bottom surface of the Fin Ray and cylinder models. Prior to each simulation, mesh convergence analysis was carried out to eliminate the influence of the element size on the results. This led to a maximum of 210 500 elements for the Fin Ray-based models.

Manufacturing of Compliant Fin Ray-Based Structures: We used the SolidWorks CAD software package to construct the Fin Ray-based structure for 3D printing. The size of the structure is shown in Figure S3, Supporting Information.

The slicing of the model was carried out using extracted mesh of 1 mm grid size. Two different materials were used. One was the FilaFlex filament material (which was a thermoplastic elastomer [TPE] with a polyurethane base with some additives) to create the compliant Fin Ray-based structure.

Another was the standard polylactic acid (PLA) filament material to create the plastic connector of the structure for fixing to the robot leg. It was decided to 3D print this whole part with dual extrusion, such that the final component would be in one piece with no additional gluing needed. When PLA was added on top of FilaFlex, it did not fuse well, although this was not the case when FilaFlex was fused on top of PLA. Consequently, to create a firm and stable connection between the two filaments, we designed the structure in a way that, on each layer or slice, FilaFlex was always fused on top of PLA. The main problem with fusing the two materials was that PLA uses a lower temperature than FilaFlex which was why PLA did not fuse into it. The model was sliced such that it was printed from the side up, to minimize the use of support in the process. Printing from the side up also ensured that the crossbeam angles of the Fin Ray-based structure do not differ significantly from the physical model compared with the CAD design. To support this print, PLA was used in a nondense structure, making it easier to remove after completion of the printing process. The final result is shown in Figure S3, Supporting Information.

Bio-Inspired Robot Leg with a Fin Ray-Based Foot: The robot leg used in this study was a biologically inspired hardware platform (Figure 8a) which was developed in our previous work.^[5] The leg, which was a simplified version of a hind leg of a dung beetle (Figure 8b), consisted of three active joints (TC, CF, and FT; three degrees of freedom (DOFs)) and three segments (coxa, femur, and tibia). The TC joint connected the thorax and coxa segments, whereas the CF joint connected the coxa and femur segments and the FT joint connected the femur and tibia segments (Figure 8a).

The compliant robot foot with a Fin Ray-based structure was attached to the end of the tibia segment. The lengths of the leg segments were designed by following the proportion of the dung beetle hind leg. All segments were produced using 3D printing. The CF and FT joints rotated around the y -axis to enable elevation and depression as well as extension and flexion of the leg, whereas the TC joint rotated around the x axis to enable forward and backward movements of the leg (Figure 8a). These movements followed the joint rotations of the real dung beetle leg. The TC joint was driven by the Hitec HS645MG servo motor with a maximum torque of 10.0 kg cm and the CF and FT joints were driven by the Hitec HS85MG micro servo motors with a maximum torque of 3.5 kg cm. The main reason for using different servo motors was to balance between the torque and length of the segments and kept the entire leg at a minimal size. The total weight of the leg including the foot was ≈ 275 g or 2.7 N. The base of the TC joint was attached to a linear slide which can be considered as the body part or the thorax. This allowed the leg to freely move in a vertical direction along the z -axis (Figure 8a). A flexible cable was used to hold the leg during a swing phase for ground clearance. This mimics the action of other legs which were not implemented in the current setup. All servo motors were driven by the output signals of neural control (Figure 8c) through the Multi-Servo IO-Board (MBoard). The MBoard was interfaced with a personal computer (PC) via an RS232 serial connection at 57.6 kbits s^{-1} .

Bio-Inspired Hexapod Robot with Fin Ray-Based Feet: The hexapod robot used in this study was a biologically inspired hardware platform (Figure 8d) which was developed based on the modular robot framework (MORF),^[44] reproduced under a research collaboration between the University of Southern Denmark (SDU) and Vidyasirimedhi Institute of Science and Technology (VISTEC). The robot had six identical legs, each of which had three active joints (TC, CF, and FT; three DOFs) and three segments (coxa, femur, and tibia). The TC joint enabled forward and backward leg movements, the CF joint enabled elevation and depression of the leg, and the FT joint enabled extension and flexion of the tibia. The robot had in total 18 active joints. They were driven by the digital servo motors (Dynamixel XM430-W350-R by Robotis). Each motor produced a maximum torque of around 48 kg cm and provided proprioceptive feedback (joint angle and torque). All servo motors were driven by the output signals of neural control (Figure 8e) through the digital motion processor (DMP) controller board. The board was interfaced with a PC via a universal serial bus (USB) connection. The weight of the fully equipped robot (including 18 motors, all electronic components, and battery packs) was ≈ 4 kg or 39 N (for more details on the robot, see the study by Thor et al.^[44]).

Neural Locomotion Control: Neural control for locomotion generation of the bio-inspired single robot leg and hexapod robot was developed in our

previous work.^[5,45] Here, we used it for our robot experiments without any modification and sensory feedback. For controlling the single leg, the control (Figure 8c) consisted of a neural central pattern generator (CPG) module for basic rhythmic pattern generation and a CPG postprocessing module for CPG signal shaping to obtain proper leg movements (Figure 5). We only used the periodic output of the neuron N_1 to directly control the TC joint (Figure 5b) and indirectly control the CF joint via the CPG postprocessing module (Figure 5c). The FT joint was set to a certain angle (Figure 5d). For controlling the hexapod robot, the control (Figure 8e) consisted of the same CPG module for basic rhythmic pattern generation, the same CPG postprocessing module for CPG signal shaping to obtain proper leg movements, and an additional premotor network module for leg coordination and wave gait generation (Figure S1, Supporting Information). We used the periodic outputs of the neurons $N_{1,2}$ indirectly control all joints via the CPG postprocessing and premotor network modules.

For both robots, the CPG module is realized using the discrete-time dynamics of a simple two-neuron recurrent network. The activity a_i of each neuron N_i develops according to

$$a_i(t) = \sum_{j=1}^n W_{ij} o_j(t-1), \quad i = 1, \dots, n \quad (1)$$

where n denotes the number of neurons (in this case, $n = 2$). W_{ij} is the synaptic strength of the connection from neuron j to neuron i . Here, we set the synaptic strength to $W_{11} = 0.98$, $W_{21} = 0.25$, $W_{12} = -0.25$, and $W_{22} = 0.98$ for the single leg robot control, and $W_{11} = 1.4$, $W_{21} = 0.19$, $W_{12} = -0.19$, and $W_{22} = 0.88$ for the hexapod robot control. This setup can generate stable rhythmic patterns for robot locomotion on the tubes. The outputs $o_{1,2}$ of the neurons $N_{1,2}$ were calculated using the hyperbolic tangent (tanh) transfer function, i.e., $o_{1,2} = \tanh(a_{1,2})$, $\in [-1, 1]$. For the single-leg robot, the CPG postprocessing module is realized by a simple clipping function. It basically passed the ascending CPG signal to rotate the CF joint to swing the leg and set the descending CPG signal to a fixed value to keep the CF joint at a certain position during the stance phase (Figure 5c). For the hexapod robot, the CPG postprocessing module was also realized by a simple clipping function. However, in this case, it passed two ascending CPG signals through the premotor network module to finally rotate the CF and FT joints to swing the leg and set the descending CPG signals to fixed values to keep the CF and FT joints at certain positions during the stance phase (Figure S1, Supporting Information). The premotor network module was a modular feedforward neural network that distributed the shaped CPG signals to all joints and formed a wave gait (for more details see the studies by Manoonpong and coworkers^[45,46]). With this simple control strategy, the neural locomotion control acts as an open-loop control system to drive the robots for on-pipe walking.

Supporting Information

Supporting Information is available from the Wiley Online Library or from the author.

Acknowledgements

This research was supported by the Startup Grant-IST Flagship research of VISTEC on Bio-inspired Robotics and the Human Frontier Science Program (grant no. RGP0002/2017). This work was partially funded by the German Science Foundation (Deutsche Forschungsgemeinschaft (DFG) grant GO 995/38-1).

Conflict of Interest

The authors declare no conflict of interest.

Authors Contribution

P.M. and H.R. contributed equally to this work. P.M., H.R., and S.N.G. worked out the conception of the study as well as conceived and designed the experiments. P.M. developed the single-leg robot system and neural control, performed single leg experiments, and data analysis. H.R., S.S.R., and A.D. carried out FEA-based numerical simulation and analysis. J.C.L. developed the physical Fin Ray models. H.T.T. carried out the tests of the physical models. N.A. and J.H. printed Fin Ray models and installed them on the hexapod robot and robot arm. P.M., N.A., and J.H. carried out hexapod robot and gripper experiments. The manuscript was written by P.M., H.R., J.C.L., and S.N.G. and then discussed and reviewed by all authors. P.M., J.C.L., and S.N.G. obtained the funding from the Human Frontier Science Program and P.M. obtained the funding from Vidyasirimedhi Institute of Science and Technology (VISTEC). S.N.G. obtained the funding from the German Science Foundation (DFG).

Data Availability Statement

The data that support the findings of this study are available from the corresponding author upon reasonable request.

Keywords

biomechanical structures, morphological computation, pipe inspection robots, soft foot, walking robots

Received: July 1, 2021
Revised: September 1, 2021
Published online:

- [1] O. Pfaff, S. Simeon, C. Ivan, S. Pavol, in *Annals of DAAAM for 2011 and Proc. of the 22nd Inter. DAAAM Symp.*, DAAAM International, Vienna, Austria, EU **2011**, pp. 1247–1249.
- [2] B. R. Aiello, A. R. Hardy, C. Cherian, A. M. Olsen, S. E. Ahn, M. E. Hale, M. W. Westneat, *J. Exp. Biol.* **2018**, 221, 1.
- [3] Festo, Multichoicегripper, <https://www.festo.com/group/en/cms/10221.htm> (accessed: September 2021) (2014).
- [4] Festo, Aquajelly, <https://www.festo.com/group/en/cms/10227.htm> (accessed: September 2021) (2013).
- [5] G. Di Canio, S. Stoyanov, J. C. Larsen, J. Hallam, A. Kovalev, T. Kleinteich, S. Gorb, P. Manoonpong, *Artif. Life Rob.* **2016**, 21, 274.
- [6] W. Crooks, S. Rozen-Levy, B. Trimmer, C. Rogers, W. Messner, *Int. J. Adv. Rob. Syst.* **2017**, 14, 1729881417721155.
- [7] S. Michel, C. Jordi, L. Wahl, N. Widmer, E. Fink, L. Kniese, A. Bormann, *Proc. of the 19th International Conf. on Adaptive Structures and Technologies*, Swiss Federal Laboratories for Materials Science and Technology (Empa), Ascona, Switzerland, October 6–9, **2008**, pp. 489–509, <http://toc.proceedings.com/09421webtoc.pdf>.
- [8] W. Crooks, G. Vukasin, M. O'Sullivan, W. Messner, C. Rogers, *Front. Rob. AI* **2016**, 3, 70.
- [9] V. Tharayil, E. Babu, A. Cherussery, J. Joy, *SSRG Int. J. Mech. Eng.* **2017**, 42.
- [10] C. I. Basson, G. Bright, in *Proc. of the 15th Inter. Conf. on Informatics in Control, Automation and Robotics*, SCITEPRESS, Portugal **2018**, pp. 81–90.
- [11] C. I. Basson, G. Bright, A. J. Walker, *S. Afr. J. Ind. Eng.* **2018**, 29, 128.
- [12] P. Borjindakul, N. Jinuntuya, A. Drimus, P. Manoonpong, in *Inter. Conf. on Simulation of Adaptive Behavior*, Springer Nature, Switzerland **2018**, pp. 136–146.
- [13] X. Shan, L. Birglen, *Int. J. Rob. Res.* **2020**, 39, 1686, <https://doi.org/10.1177/0278364920913926>.
- [14] R. Chen, R. Song, Z. Zhang, L. Bai, F. Liu, P. Jiang, D. Sindersberger, G. J. Monkman, J. Guo, *Soft Rob.* **2019**, 6, 701.
- [15] K. Elgeneidy, A. Fansa, I. Hussain, K. Goher, in *2020 3rd IEEE Inter. Conf. on Soft Robotics (RoboSoft)*, IEEE, Piscataway, NJ **2020**, pp. 779–784.
- [16] S. Gorb, M. Scherge, *Proc. R. Soc. London, Ser. B* **2000**, 267, 1239.
- [17] S. Gorb, Y. Jiao, M. Scherge, *J. Comp. Physiol. A* **2000**, 186, 821.
- [18] R. G. Beutel, S. Gorb, *J. Zool. Syst. Evol. Res.* **2001**, 39, 177.
- [19] V. V. Ernst, *Tissue Cell* **1973**, 5, 83.
- [20] G. Hanna, W. Jon, W. P. Jon Barnes, *J. Exp. Biol.* **1991**, 155, 103.
- [21] J. Schaffer, *Z. Wiss. Zool.: Abt. A* **1905**, 83, 231.
- [22] J. G. M. Thewissen, S. A. Etnier, *J. Mammal.* **1995**, 76, 925.
- [23] P. Flammang, *Echinoderm Stud.* **1996**, 5, 1.
- [24] R. Santos, S. Gorb, V. Jamar, P. Flammang, *J. Exp. Biol.* **2005**, 208, 2555.
- [25] B. N. J. Persson, S. Gorb, *J. Chem. Phys.* **2003**, 119, 11437.
- [26] C.-Y. Hui, N. J. Glassmaker, A. Jagota, *J. Adhes.* **2005**, 81, 699.
- [27] S. Gorb, *Attachment Devices of Insect Cuticle*, Springer Nature, Switzerland **2001**.
- [28] M. Schargott, V. L. Popov, S. Gorb, *J. Theor. Biol.* **2006**, 243, 48.
- [29] P. Gregorio, M. Ahmadi, M. Buehler, *IEEE Trans. Syst. Man Cybern. B Cybern.* **1997**, 27, 626.
- [30] P. Manoonpong, T. Kulvicius, F. Wörgötter, L. Kunze, D. Renjewski, A. Seyfarth, in *2011 11th IEEE-RAS Inter. Conf. on Humanoid Robots*, IEEE, Piscataway, NJ **2011**, pp. 276–281.
- [31] F. P. Bowden, D. Tabor, *The Friction and Lubrication of Solids*, Clarendon Press, Oxford, OX **1986**.
- [32] K. Duvefelt, *Ph.D. Thesis*, KTH Royal Institute of Technology, **2016**.
- [33] R. Sahli, G. Pallares, C. Ducottet, I. B. Ali, S. Al Akhrass, M. Guibert, J. Scheibert, *Proc. Natl. Acad. Sci.* **2018**, 115, 471.
- [34] S. Bartsch, T. Birnschein, F. Cordes, D. Kuehn, P. Kampmann, J. Hilljegerdes, S. Planthaber, M. Roemmermann, F. Kirchner, in *ISR 2010 (41st Inter. Symp. on Robotics) and ROBOTIK 2010 (6th German Conf. on Robotics)*, VDE, Berlin **2010**, pp. 1–8.
- [35] S. Ohtsuka, G. Endo, E. F. Fukushima, S. Hirose, in *2010 IEEE/RSJ Inter. Conf. on Intelligent Robots and Systems*, IEEE, Piscataway, NJ **2010**, pp. 5354–5359.
- [36] S. Hauser, M. Mutlu, P. Banzet, A. J. Ijspeert, *Adv. Rob.* **2018**, 32, 825.
- [37] L. Paez, K. Melo, R. Thandiackal, A. J. Ijspeert, in *2019 2nd IEEE Inter. Conf. on Soft Robotics (RoboSoft)*, IEEE, Piscataway, NJ **2019**, pp. 178–185.
- [38] D. Voigt, A. Karguth, S. Gorb, *Rob. Auton. Syst.* **2012**, 60, 1046.
- [39] H. T. Tramsen, A. E. Filippov, S. N. Gorb, L. Heepe, *Adv. Mater. Interfaces* **2020**, 7, 1901930.
- [40] D. Gladun, S. N. Gorb, *Arthropod-Plant Interact.* **2007**, 1, 77.
- [41] R. Pfeifer, J. Bongard, *How the Body Shapes the Way We Think: A New View of intelligence*, MIT press, Cambridge, MA **2006**.
- [42] H. Hauser, A. J. Ijspeert, R. M. Fuchslin, R. Pfeifer, W. Maass, *Biol. Cybern.* **2011**, 105, 355.
- [43] K. A. Daltorio, A. D. Horchler, S. Gorb, R. E. Ritzmann, R. D. Quinn, in *2005 IEEE/RSJ Inter. Conf. on Intelligent Robots and Systems*, IEEE, Piscataway, NJ **2005**, pp. 3648–3653.
- [44] M. Thor, J. C. Larsen, P. Manoonpong, in *Proc. 2nd Int. Youth Conf. Bionic Eng. (IYCBE)*, Frontiers, Switzerland **2018**, pp. 23–25.
- [45] P. Manoonpong, U. Parlitz, F. Wörgötter, *Front. Neural Circuits* **2013**, 7, 12.
- [46] E. Grinke, C. Tetzlaff, F. Wörgötter, P. Manoonpong, *Front. Neurobot.* **2015**, 9, 11.